

LETTER • OPEN ACCESS

Green-wavelength GaN-based photonic-crystal surface-emitting lasers

To cite this article: Natsuo Taguchi *et al* 2024 *Appl. Phys. Express* **17** 012002

View the [article online](#) for updates and enhancements.

You may also like

- [High-power, stable single-mode CW operation of 1550 nm wavelength InP-based photonic-crystal surface-emitting lasers](#)
Takeshi Aoki, Yuhki Itoh, Kosuke Fujii et al.
- [Photonic-crystal lasers with high-quality narrow-divergence symmetric beams and their application to LiDAR](#)
Masahiro Yoshida, Menaka De Zoysa, Kenji Ishizaki et al.
- [Transverse dynamics in cavity nonlinear optics \(2000–2003\)](#)
Paul Mandel and M Tlidi



Green-wavelength GaN-based photonic-crystal surface-emitting lasers

Natsuo Taguchi^{1,2*}, Akinori Iwai^{1,2}, Masahiro Noguchi¹, Hiroaki Takahashi^{1,2}, Atsuo Michiue^{1,2}, Menaka De Zoysa³, Takuya Inoue³, Kenji Ishizaki³, and Susumu Noda^{2,3}

¹Nichia Research Institute, Nichia Corporation, Anan, Tokushima 774-8601, Japan

²Department of Electronic Science and Engineering, Kyoto University, Kyoto 615-8510, Japan

³Photonics and Electronics Science and Engineering Center, Kyoto University, Kyoto 615-8510, Japan

*E-mail: natsuo.taguchi@nichia.co.jp

Received October 13, 2023; revised December 3, 2023; accepted December 5, 2023; published online January 3, 2024

Visible-wavelength GaN-based photonic-crystal surface-emitting lasers (PCSELS) have attracted attention for various applications, such as materials processing, high-brightness illuminations, and displays. In this letter, we demonstrate GaN-based PCSELS at green wavelengths. We formed a photonic crystal (PC) in p-GaN and filled holes of the PC with SiO₂ to ensure device stability. Through a current injection test under pulsed conditions and spectral analysis, we confirmed that the fabricated device possessed Γ -point single-mode oscillation at wavelengths above 505 nm. Our results have the potential to further expand the applications of PCSELS and semiconductor lasers in visible region.

© 2024 The Author(s). Published on behalf of The Japan Society of Applied Physics by IOP Publishing Ltd

Green-wavelength lasers have consistently been in high demand in areas such as displays, bioscience, and medicine. Traditionally, YAG-based lasers with second harmonic generation or He–Ne lasers have been utilized in this wavelength range. While these solid-state/gas lasers excel in beam quality, they suffer from high power consumption due to their low wall-plug efficiency (WPE) and lack portability due to their bulky size. In contrast, GaN-based visible-wavelength semiconductor lasers have the advantage of low power consumption due to their high WPE, and compact size. Since GaN-based edge-emitting laser diodes (EELDs) were first confirmed to oscillate in 1995,¹ their characteristics have improved over the years,^{2,3} including the expansion of their lasing wavelengths to ranges from green^{4,5} to ultra-violet.^{6–9} Recently, the output power of the EELDs with a center wavelength of 532 nm has reached 1.64 W.³ However, the EELDs have several problems, such as multimode oscillation in both longitudinal and transverse directions, as well as wide divergence of radiation beams and catastrophic optical damage (COD) derived from the small cross section of the ridge. GaN-based vertical-cavity surface-emitting lasers (VCSELs) have also been developed because of their attractive features, such as low threshold oscillation due to their small resonator volume, the possibility of integration, and vertical single-mode operation with a distributed Bragg reflector (DBR).^{10–14} However, when the area of the resonator is enlarged to increase the output power, the VCSELs are more likely to exhibit lateral multimode oscillation.

Photonic-crystal surface-emitting lasers (PCSELS), which employ a two-dimensional photonic crystal (PC) as a cavity, have the potential to overcome the above issues of the EELDs and the VCSELs.^{15,16} By utilizing a singularity (e.g. Γ) point of the PC, the PCSELS realize both vertical and lateral single-mode oscillation and low divergence radiation beams with angles of less than 0.2°. In addition, the light density in the resonator can be kept small even under high power because of the large resonator area, thus removing the risk of COD. Recently, double-lattice PCs, which consist of two overlapping lattice groups, have been attracting attention.¹⁷ The double-

lattice PCs allow detailed control of the interference of both 180° and 90° diffractions in the PC plane (Hermitian), as well as the interference of those diffracted lights with perpendicular radiation (non-Hermitian).¹⁸ These interference controls enable CW-driven vertical and lateral single-mode oscillation with over 50 W output power even when the resonator diameter is 3 mm.¹⁹ GaN-based PCSELS in the visible region have been developed by some groups since the first oscillation in 2008.^{20,21} Recently, CW operation at room temperature was successfully achieved using a structure in which a double-lattice PC formed in an n-GaN layer is embedded by regrowth.²² These were all achieved at blue wavelengths. One of our next goals is to extend our PCSEL platform to green wavelengths. In this study, we realize GaN-based PCSELS oscillating at green wavelengths. We have fabricated a double-lattice PC in a p-GaN layer and filled the holes of the PC with SiO₂. Here we first describe the structure of the fabricated PCSEL device. Next, we demonstrate that the device exhibits vertical and lateral single-mode oscillation at a wavelength of 505.7 nm. Finally, we show that the oscillation wavelength can be tuned in the range from approximately 505–520 nm by controlling the lattice constant of the PC.

Figure 1(a) shows a schematic image of the PCSEL chips in this study. We formed a PC in p-GaN above an active layer. In this case, the PC is formed in p-GaN after the active layer is grown.²³ Therefore, by knowing the actual gain wavelength of the active layer, the lattice constant a can be precisely adjusted accordingly. This is a feature which does not exist when the PC is formed on an n-GaN before the active layer is grown. With respect to the PC on the p-GaN, in addition, the holes of the PC are filled with SiO₂, which is different from previously reported PCSELS with air-hole PCs. There are some characteristics of the SiO₂ PC. First, filling with SiO₂ protects the side walls of the PC from conductive particles which cause current leakage, such as Indium Tin Oxide (ITO) and the p-electrode, leading to improving operation stability of the PCSEL chips. Second, the effective refractive index of the PC layer increases and thus the distribution of the fundamental guided mode shifts to the PC layer, which leads to an enhancement of coupling between guided light and the PC. On the other hand, filling the PC with



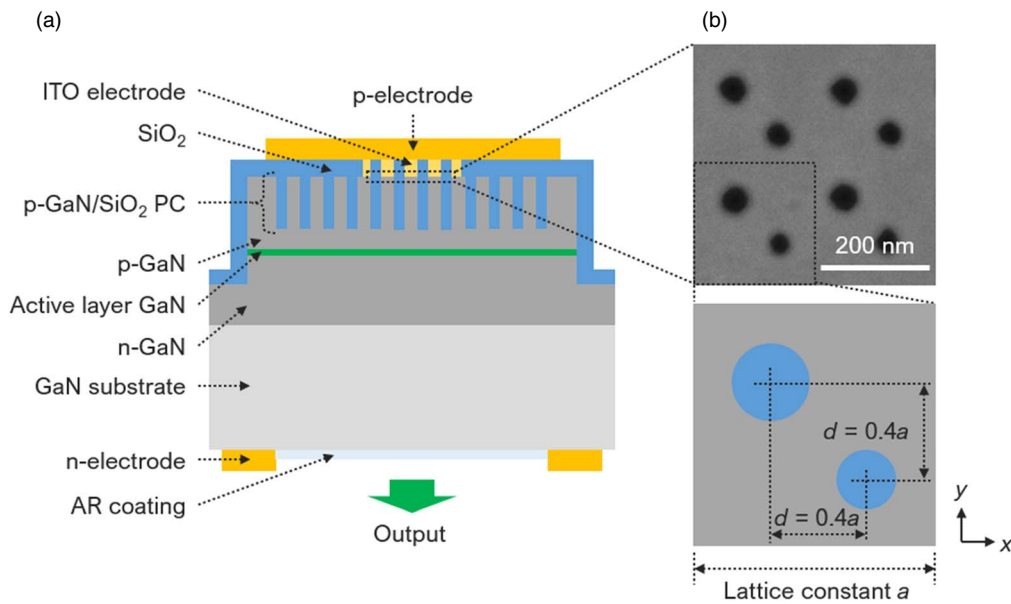


Fig. 1. Structure of green-wavelength GaN-based PCSELS. (a) Cross-sectional schematic of a diced PCSEL chip. (b) (Top) Scanning-electron-microscope image of a double-lattice p-GaN/SiO₂ PC captured at the surface of the p-GaN. Here, the ITO electrode was removed after filling the PC with SiO₂, and redundant SiO₂ was then removed to expose the surface of p-GaN. (Bottom) Schematic of the designed double-lattice PC.

SiO₂ reduces the refractive index contrast between the p-GaN and the PC compared to the case of the air-hole PC, causing a reduction of the coupling coefficients among fundamental waves propagating inside the PC layer. Note that this coupling reduction can be compensated by enlarging the filling factor (FF) of the PC. Also, we employed a double-lattice PC as shown in Fig. 1(b). Two overlapping lattice groups are separated along both the x and y directions by a distance of d with each other. In proportion to d , light diffracted in-plane by each lattice optically interferes. When $d = a/2$, the interference becomes constructive,¹⁷⁾ which strengthens in-plane optical couplings and thus in-plane optical confinement. When $d = a/4$, on the other hand, the interference becomes destructive,¹⁷⁾ which weakens the in-plane optical couplings and thus the in-plane optical confinement. In this case, higher-order in-plane modes have higher optical loss than the fundamental in-plane mode, which is suitable for a single-mode oscillation over wide resonator areas. In the present study, we set d as $0.4a$ to obtain sufficient in-plane confinement and coupling even in the case of low refractive index contrast between p-GaN and SiO₂ filling the PC.

The fabrication process of the PCSELS is described below. First, an n-GaN layer, an active layer, and a p-GaN layer were sequentially grown on a GaN substrate. An ITO film was subsequently deposited on the p-GaN layer. Next, a double-lattice PC was formed in the ITO film and the p-GaN layer using electron-beam (EB) lithography and inductively-coupled-plasma reactive-ion-etching (ICP-RIE). Next, the holes of the PC were filled with SiO₂ utilizing a plasma CVD process, and then the ITO film was removed, except for a central circular area with 300 μm diameter to be used as an electrode. Note that after filling the PC with SiO₂, a small air void was observed at the center of each hole by cross-sectional scanning-electron-microscope imaging of the PC. The shape of the void was uniform within the PC plane, and the presence of the void thus was considered not to significantly impact the behavior of the PCSEL. Afterwards, exposing the n-GaN layer, forming a SiO₂

film over the area except for the central area of ITO, depositing both a p-electrode and an n-electrode with a circular aperture for laser output, and applying an AR coating inside the circular aperture of the n-electrode were sequentially carried out. Finally, the green GaN-based PCSEL was diced and mounted on a submount in the face-down configuration.

A current injection test was performed on the fabricated green GaN-based PCSEL. Figure 2(a) shows a finished device with a lattice constant $a = 210$ nm. A circular aperture is opened in the wire-bonded n-electrode, and the ITO electrode is located at the center of the aperture. The test was under room temperature and pulsed conditions where the pulse width and the repetition frequency were 500 ns and 1 kHz, respectively. Figure 2(b) shows a near-field pattern (NFP) of the ITO electrode obtained at an injection current of 1.23 A, demonstrating that the current was confined to the ITO electrode area. The periphery of the ITO electrode area appears dark because the SiO₂ film slightly overlaps between the ITO and the p-electrode. Figure 2(c) shows the output power-current characteristic of the device. A steep increase in output power was observed at a current density threshold of ~ 3.89 kA cm⁻², demonstrating laser oscillation. A slope efficiency of ~ 0.02 W A⁻¹ was obtained. The maximum output power was ~ 50 mW at a current of ~ 5 A, with a wall-plug efficiency (WPE) of $\sim 0.1\%$. A far-field pattern (FFP) obtained at a current of 2.9 A, which is just above the lasing threshold, is shown in Fig. 2(d). The FFP was a single-lobed circular point with a narrow divergence angle, demonstrating lateral single-mode Γ -point operation. The output beam also possessed linear polarization, and the maximum (Max) and minimum (Min) output powers were observed along the polarization angle. Using the definition of the polarization ratio as $R_{\text{Pol}} = (\text{Max} - \text{Min})/(\text{Max} + \text{Min})$, the value of R_{Pol} was ~ 0.8 .

Figure 3 describes the spectral characteristics of the same PCSEL device discussed in the above section. The photonic band diagram, which is composed of spontaneous emission spectra measured at different angles from the surface of the device, is shown in Fig. 3(a). Four bands which are labeled as

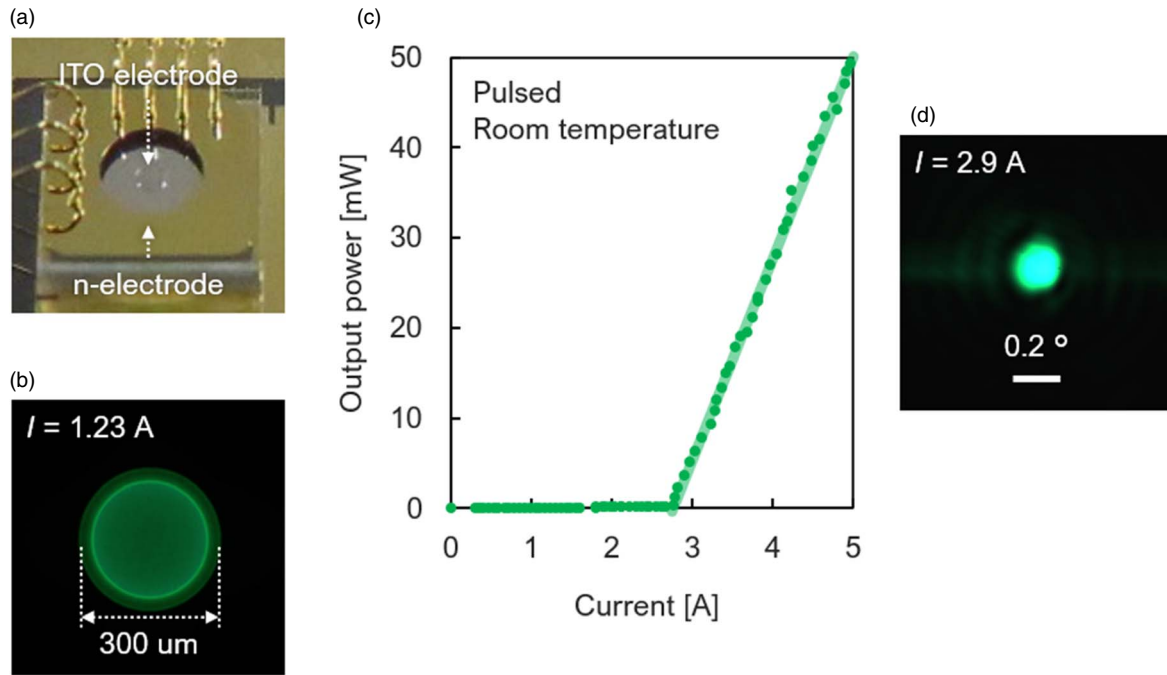


Fig. 2. Operation characteristics of a device ($a = 210$ nm) under room temperature pulsed conditions (pulse width 500 ns, repetition frequency 1 kHz). (a) Picture of a finished device in the face-down configuration. The aperture diameter of the n-electrode was $900 \mu\text{m}$. (b) Microscope image of a NFP of the ITO electrode captured at a current density of 1.43 kA cm^{-2} . (c) Output power-injection current characteristic. (d) FFP under a current density of 3.24 kA cm^{-2} .

A, B, C, and D are observed, originating from the square lattice. Figure 3(b) shows the spontaneous emission spectrum at the Γ -point of the band structure, where lasing spectra at injection currents of 4 A and 5 A are also shown. Comparison of these spectra shows that the lasing is not only in a single lateral mode, but also in a single vertical mode on band B at 505.7 nm. The coupling coefficients κ_{1D} and κ_{2D} associated with in-plane coupling at angles of 180° and 90° can be determined from the gaps of the four bands on the spontaneous emission spectra at the Γ -point.²⁴⁾ In this work, κ_{1D} and κ_{2D} of the device were determined to be 207 cm^{-1} and 11 cm^{-1} , respectively.

The lasing wavelength λ_L of the PCSELs is given by $\lambda_L = n_{\text{eff}}a$, where n_{eff} is the effective refractive index at the oscillation wavelength. In other words, the lasing wavelength can be arbitrarily tuned by the lattice constant a . Figure 4 shows lasing spectra of devices with lattice constants between 210 nm and 217 nm, varying by 1 nm with each other. It can be observed that the lasing wavelength redshifted as the lattice constant increases. In this study, lasing with a maximum wavelength of 520.5 nm was confirmed. On the other hand, the gain peak of the active layer in the present study was around 505 nm. As the lattice constant increased,

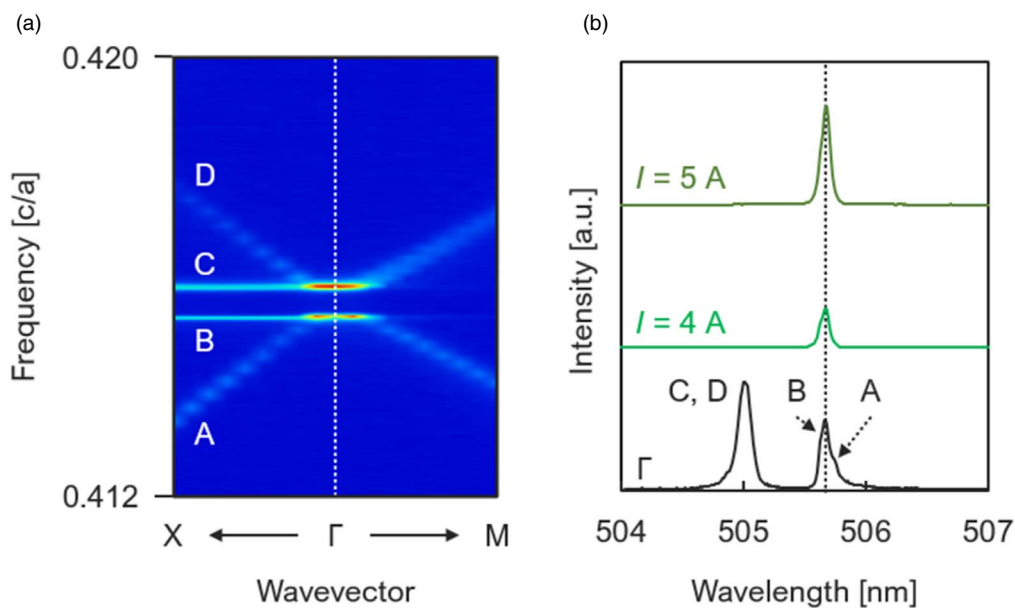


Fig. 3. Spectral characteristics. (a) Measured photonic band diagram of the device. The spectra composing the band were obtained at a current of 2.5 A, which is below the lasing threshold, and they are normalized by c/a where c is the speed of light in free space. (b) Spontaneous emission spectrum at the Γ -point (black) corresponding to the white-dotted line in (a), where lasing spectra obtained at currents of 4 A (light green) and 5 A (dark green) are imposed. The lasing spectra were obtained using an integrating sphere.

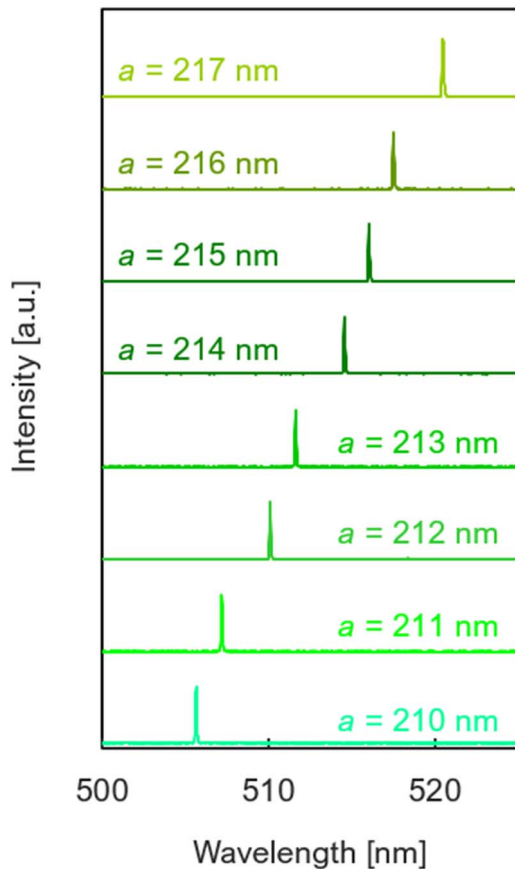


Fig. 4. Lasing spectra of devices with different lattice constants.

therefore, the lasing wavelength shifted away from the gain peak, resulting in an increase in the lasing threshold. Some of these devices also exhibited flat-band lasing with line-shaped FFPs. The flat-band lasing observed here is attributed to fluctuations in the PC structure in addition to the relatively low κ_{2D} . Structural nonuniformities in the in-plane and depth directions would lead to a reduction of κ_{2D} and thus precipitate flat-band lasing.

As demonstrated in the above current injection test and the photonic band analysis, we have successfully developed the PCSELS with single-mode Γ -point operation at green wavelengths. On the other hand, the operating characteristics as a laser diode (LD) are still at a primitive level compared with those of PCSELS at blue wavelengths²²⁾ as well as those of existing EELDs³⁾ and VCSELS at green wavelengths.¹⁴⁾ The WPE can be improved by optimizing both the PC and the epitaxial crystal layers. For the PC, stronger in-plane coupling and vertical radiation are expected to be obtained by optimizing the geometry. The epitaxial crystal layers should be designed to maximize the intensity of the fundamental guided mode in the PC region, while also considering the non-luminescent loss of injected carriers.

In conclusion, we have realized the development of GaN-based PCSELS operating at green wavelengths by utilizing a SiO₂-filled double-lattice PC formed in a p-GaN layer. The SiO₂ filling contributes to improving operation stability and coupling enhancement, but also deteriorates optical coupling, due to a decrease of refractive index contrast of the PC, which can be compensated by enlarging the filling factor. A current injection test was performed, demonstrating laser oscillation

and single-mode Γ -point operation with a maximum output power of ~ 50 mW and a WPE of $\sim 0.1\%$. A slope efficiency of ~ 0.02 W A^{-1} was obtained. By comparing the photonic band diagram and lasing spectra, we clarified that the single-mode oscillation occurred on band B at 505.7 nm. Furthermore, we were able to arbitrarily tune the lasing wavelength by the lattice constant and confirm lasing with a maximum wavelength of 520.5 nm. However, the operating characteristics as a LD, such as WPE, current threshold, and slope efficiency, are still behind those of existing LDs.^{3,14,22)} CW operation is one of the main objectives for future research. The WPE is expected to be improved by optimizing both the PC and the epitaxial crystal layers. The results presented here will expand the operating wavelength range of the PCSELS in the visible region, further enhancing their potential as LDs.

Acknowledgments This work was partially supported by the Japan Society for the Promotion of Science (Grant-in-Aid for Scientific Research 22H04915), and Council for Science, Technology and Innovation (CSTI) (Program for Bridging the Gap between R&D and the Ideal Society (Society 5.0) and Gathering Economic and Social Value (BRIDGE)).

- 1) S. Nakamura, M. Senoh, S. Nagahama, N. Iwasa, T. Yamada, T. Matsushita, H. Kiyoku, and Y. Sugimoto, *Jpn. J. Appl. Phys.* **35**, L74 (1996).
- 2) M. Z. Baten, S. Alam, B. Sikder, and A. Aziz, *Photonics* **8**, 430 (2021).
- 3) Y. Nakatsu, T. Hirao, T. Morizumi, Y. Nagao, K. Terao, H. Nagai, S. Masui, T. Yanamoto, and S. Nagahama, *Gallium Nitride Mater. Devices XVIII* **12421**, 124210F (2023).
- 4) A. Avramescu, T. Lerner, J. Müller, C. Eichler, G. Bruederl, M. Sabathil, S. Lutgen, and U. Strauss, *Appl. Phys. Express* **3**, 061003 (2010).
- 5) M. Murayama, Y. Nakayama, K. Yamazaki, Y. Hoshina, H. Watanabe, N. Fuitagawa, H. Kawanishi, T. Uemura, and H. Narui, *Phys. Status Solidi (a)* **215**, 1700513 (2018).
- 6) S. Nagahama, T. Yanamoto, M. Sano, and T. Mukai, *Jpn. J. Appl. Phys.* **40**, L785-7 (2001).
- 7) M. Kneissl, D. W. Treat, M. Teepe, N. Miyashita, and N. M. Johnson, *Appl. Phys. Lett.* **82**, 4441 (2003).
- 8) Z. Zhang, M. Kushimoto, T. Sakai, N. Sugiyama, L. J. Schowalter, C. Sasaoka, and H. Amano, *Appl. Phys. Express* **12**, 124003 (2019).
- 9) T. Omori et al., *Appl. Phys. Express* **13**, 071008 (2020).
- 10) T.-C. Lu, C.-C. Kao, H.-C. Kuo, G.-S. Huang, and S.-C. Wang, *Appl. Phys. Lett.* **92**, 141102 (2008).
- 11) Y. Higuchi, K. Omae, H. Matsumura, and T. Mukai, *Appl. Phys. Express* **1**, 121102 (2008).
- 12) M. Kuramoto, S. Kobayashi, T. Akagi, K. Tazawa, K. Tanaka, K. Nakata, and T. Saito, *Appl. Phys. Express* **12**, 091004 (2019).
- 13) T. Hamaguchi et al., *Appl. Phys. Express* **13**, 041002 (2020).
- 14) K. Terao, H. Nagai, D. Morita, S. Masui, T. Yanamoto, and S. Nagahama, *Gallium Nitride Mater. Devices XVI* **11686**, 116860E (2021).
- 15) M. Imada, S. Noda, A. Chutinan, T. Tokuda, M. Murata, and G. Sasaki, *Appl. Phys. Lett.* **75**, 316 (1999).
- 16) S. Noda, K. Kitamura, T. Okino, D. Yasuda, and Y. Tanaka, *IEEE J. Sel. Top. Quantum Electron.* **23**, 1 (2017).
- 17) M. Yoshida, M. D. Zoysa, K. Ishizaki, Y. Tanaka, M. Kawasaki, R. Hatsuda, B. Song, J. Gellata, and S. Noda, *Nat. Mater.* **18**, 121 (2019).
- 18) T. Inoue, M. Yoshida, J. Gellata, K. Izumi, K. Yoshida, K. Ishizaki, M. D. Zoysa, and S. Noda, *Nat. Commun.* **13**, 3262 (2022).
- 19) M. Yoshida, S. Katsuno, T. Inoue, J. Gellata, K. Izumi, M. D. Zoysa, K. Ishizaki, and S. Noda, *Nature* **618**, 727 (2023).
- 20) H. Matsubara, S. Yoshimoto, H. Saito, Y. Jianglin, Y. Tanaka, and S. Noda, *Science* **319**, 445 (2008).
- 21) S. Kawashima, T. Kawashima, Y. Nagatomo, Y. Hori, H. Iwase, T. Uchida, K. Hoshino, A. Numata, and M. Uchida, *Appl. Phys. Lett.* **97**, 25112251112 (2010).
- 22) K. Emoto, T. Koizumi, M. Hirose, M. Jutori, T. Inoue, K. Ishizaki, M. D. Zoysa, H. Togawa, and S. Noda, *Commun. Mater.* **3**, 72 (2022).
- 23) L.-R. Chen, K.-B. Hong, K.-C. Huang, H.-T. Yen, and T.-C. Lu, *Opt. Express* **29**, 11293 (2021).
- 24) Y. Liang, C. Peng, K. Sakai, S. Iwahashi, and S. Noda, *Phys. Rev. B* **84**, 195119 (2011).